adjusted in each fraction to either 115 or 100 mM for the 5-HT_{2C}R and GluR-B substrates, respectively.

Pharmacological characterization. For analysis of phosphoinositide hydrolysis, transfected cells were plated in DMEM medium containing 10% calf serum, penicillin and streptomycin; 24 h after electroporation, cells were labelled overnight with 2 μCi [^{3}H]myo-inositol/ml in serum-free, inositol-free DMEM. Before addition of 5-HT, cells were washed with serum-free medium and the accumulated ^{3}H-inositol monophosphate assayed[28]. Competition binding with [^{3}H]mesulergine (1 mM) (Fig. 3b) was done as described[29] and nonspecific binding was determined with 10 μM methysergide. Apparent K_i values were calculated according to ref. 30. Published 5-HT_{2C}R (INI) K_i values were used for clozapine, mesulergine, bromo-LSD and mianserin[29]. 1.6 μM PBZ decreased receptor density to 29.6% of control (Fig. 5c), as determined by saturation binding of [^{3}H]mesulergine. EC_{50}, E_{max} and B_{max} values ($n = 3$) for PBZ-treated INI and VSV isoforms were 6.6 ± 2.5 nM compared with 8.5 ± 3.7 nM, 320 ± 10 compared with 240 ± 20 per cent of basal, and 3,444 ± 448 compared with 946 ± 227 fmol per mg protein, respectively.

Received 22 August 1996; accepted 7 March 1997.

1. Hoyer, D. *et al.* IUP classification of receptors for 5-hydroxytryptamine (serotonin). *Pharmacol. Rev.* **46,** 157–203 (1994).
2. Polson, A. G., Bass, B. L. & Casey, J. L. RNA editing of hepatitis delta virus antigenome by dsRNA-adenosine deaminase. *Nature* **380,** 454–456 (1996).
3. Sommer, B., Kohler, M., Sprengel, R. & Seeburg, P. H. RNA editing in brain controls a determinant of ion flow in glutamate-gated channels. *Cell* **67,** 11–19 (1991).
4. Lomeli, H. *et al.* Control of kinetic properties of AMPA receptor channels by nuclear RNA editing. *Science* **266,** 1709–1713 (1994).
5. Kohler, M., Burnashev, N., Sakmann, B. & Seeburg, P. Determinants of Ca^{2+} permeabiity in both TM1 and TM2 of high affinity kainate receptor channels: diversity by RNA editing. *Neuron* **10,** 491–500 (1993).
6. Egebjerg, J. & Heinemann, S. F. Intron sequence directs RNA editing of the glutamate receptor subunit GluR2 coding sequence. *Proc. Natl Acad. Sci. USA* **90,** 755–759 (1993).
7. Zuker, M. Computer prediciton of RNA structure. *Meth. Enzymol.* **180,** 262–288 (1989).
8. Higuchi, M. *et al.* RNA editing of AMPA receptor subunit GluR-B: a base-paired intron–exon structure determines positon and efficiency. *Cell* **75,** 1361–1370 (1993).
9. Herb, A., Higuchi, M., Sprengel, R. & Seeburg, P. H. Q/R site editing in kainate receptor GluR5 and GluR6 pre-mRNAs requires distant intronic sequences. *Proc. Natl Acad. Sci. USA* **93,** 1875–1880 (1996).
10. Rueter, S. *et al.* Glutamate receptor RNA editing *in vitro* by enzymatic conversion of adenosine to inosine. *Science* **267,** 1491–1494 (1995).
11. Yang, J.H., Sklar, P., Axel, R. & Maniatis, T. Editing of glutamate receptor subunit B pre-mRNA *in vitro* by site-specific deamination of adenosine. *Nature* **374,** 77–81 (1995).
12. Maas, S. *et al.* Structural requirements for RNA editing in glutamate receptor pre-mRNAs by recombinant double-stranded RNA adenosine deaminase. *J. Biol. Chem.* **271,** 12221–12226 (1996).
13. Melcher, T. *et al.* A mammalian RNA editing enzyme. *Nature* **379,** 460–464 (1996).
14. Bass, B. RNA editing: New uses for old players in the RNA world. *The RNA World* 383–418 (Cold Spring Harbor Laboratory Press, New York, 1993).
15. Gomeza, J. *et al.* The second intracellular loop of metabotropic glutamate receptor 1 cooperates with the other intracellular domains to control coupling to G-proteins. *J. Biol. Chem.* **271,** 2199–2205 (1996).
16. Westphal, R. S., Backstrom, J. R. & Sanders-Bush, E. Increased basal phosphorylation of the constitutively active serotonin 2C receptor accompanies agonist-mediated desensitization. *Mol. Pharmacol.* **48,** 200–205 (1995).
17. Ariëns, E. J., Beld, A. J., Rodrigues de Miranda, J. F. & Simonis, A. M. *The Receptors* 33–91 (Plenum, New York, 1979).
18. Meller, E. *et al.* Receptor reserve for D2 dopaminergic inhibition of prolactin release *in vivo* and *in vitro*. *J. Pharmacol. Exp. Ther.* **257,** 668–675 (1991).
19. Leonhardt, S., Garospe, E., ,Hoffman, B. J. & Teitler, M. Molecular pharmacological differences in the interaction of serotonin with 5-hydroxytryptamine 1C and 5-hydroxytryptamine2 receptors. *Mol. Pharmacol.* **42,** 328–335 (1992).
20. Ross, E. M. G protein GTPase-activating proteins: regulation of speed, amplitude, and signaling selectivity. *Rec. Prog. Horm. Res.* **50,** 207–221 (1995).
21. Moro, O., Lameh, J., Högger, P. & Sadée, W. Hydrophobic amino acid in the i2 loop plays a key role in receptor–G protein coupling. *J. Biol. Chem.* **268,** 22273–22276 (1993).
22. Yu, L. *et al.* The mouse 5-HT1C receptor contains eight hydrophobic domains and is X-linked. *Mol. Brain Res.* **11,** 143–149 (1991).
23. Kennelly, P. J. & Krebs, E. G. Consensus sequences as substrate specificity determinants for protein kinases and protein phosphatases. *J. Biol. Chem.* **266,** 15555–15558 (1991).
24. Julius, D., MacDermott, A. B., Axel, R. & Jessell, T. M. Molecular characterization of a functional cDNA encoding the serotonin 1c receptor. *Science* **241,** 558–264 (1988).
25. Ausubel, F. *et al.* (eds) Current Protocols in Molecular Biology (Wiley, New York, 1989).
26. O'Connell, M. *et al.* Cloning of cDNAs encoding mammalian double-stranded RNA-specific adenosine deaminase. *Mol. Cell. Biol.* **15,** 1389–1397 (1995).
27. Gorski, K., Carneiro, M. & Schibler, U. Tissue-specific *in vitro* transcription from the mouse albumin promoter. *Cell* **47,** 767–776 (1986).
28. Barker, E. L., Westphal, R. S., Schmidt, D. & Sanders-Bush, E. Constitutively active 5-hydroxytryptamine2C receptors reveal novel inverse agonist activity of receptor ligands. *J. Biol. Chem.* **269,** 11687–11690 (1994).
29. Westphal, R. S. & Sanders-Bush, E. Reciprocal binding properties of 5-hydroxytryptamine type 2C receptor agonists and inverse agonists. *Mol. Pharmacol.* **46,** 937–942 (1994).
30. Cheng, Y. & Prusoff, W. H. Relationship between the inhibiton constant (K_i) and the concentration of inhibitor which causes 50 per cent inhibition (IC_{50}) of enzymatic reaction. *Biochem. Pharmacol.* **22,** 3099–3108 (1973).

Acknowledgements. We thank B. Wadzinski for assistance with biochemical fractionation analysis, J. Exton, J. Barnett and J. Patton for critical reading of this manuscript, and A. Westphal and A. Poindexter for their technical expertise. This work was supported by grants from the NIH, the National Defense Medical Center, Taipei, Taiwan, and the Pharmaceutical Manufacturers Association Foundation, Inc.

Correspondence and requests for materials should be addressed to R.B.E. (e-mail: ron.emeson@mcmail.vanderbilt.edu).

Elasticity and unfolding of single molecules of the giant muscle protein titin

L. Tskhovrebova*†, J. Trinick*, J. A. Sleep‡ & R. M. Simmons‡

* *Muscle Research Group, Department of Veterinary Clinical Science, Bristol University, Langford, Bristol BS18 7DY, UK*
‡ *MRC Muscle & Cell Motility Unit, Randall Institute, King's College London, 26–29 Drury Lane, London WC2B 5RL, UK*

The giant muscle protein titin, also called connectin, is responsible for the elasticity of relaxed striated muscle, as well as acting as the molecular scaffold for thick-filament formation[1,2]. The titin molecule consists largely of tandem domains of the immunoglobulin and fibronectin-III types, together with specialized binding regions and a putative elastic region, the PEVK domain[3]. We have done mechanical experiments on single molecules of titin to determine their visco-elastic properties, using an optical-tweezers technique. On a fast (0.1s) timescale titin is elastic and force–extension data can be fitted with standard random-coil polymer models, showing that there are two main sources of elasticity: one deriving from the entropy of straightening the molecule; the other consistent with extension of the polypeptide chain in the PEVK region. On a slower timescale and above a certain force threshold, the molecule displays stress-relaxation, which occurs in rapid steps of a few piconewtons, corresponding to yielding of internal structures by about 20 nm. This stress-relaxation probably derives from unfolding of immunoglobulin and fibronectin domains.

Relaxed striated muscle possesses markedly nonlinear visco-elastic properties, including stress-relaxation and hysteresis. The steady-state force–extension relationship is at first roughly exponential, but at extreme stretch there is a yield point, after which the curve is less steep. Elasticity derives principally from connections between the ends of thick filaments and the Z-line (Fig. 1a). These connections are formed by the I-band region of the roughly 3,000K protein titin; the end-to-end length of this region increases with muscle stretch, from about zero to 1 μm. The remaining (A-band) region of the titin molecule, 0.8 μm long, runs to the M-line and is normally integral with the thick filament. The maximum passive (yield) force per thick filament is in the range 100–200 pN, with between 3 and 6 titin molecules in each half filament, so the maximum force per molecule lies between 15 and 70 pN. The major part of skeletal muscle titin consists of 140–160 immunoglobulin domains and 132 fibronectin-III domains; in the I-band region the 1,000–2,200 residues of the so-called PEVK region are flanked by 70–90 immunoglobulin domains, depending on isoform[3]. Recent studies of epitope positions in preparations of stretched muscle fibres[4,5] suggest that titin has two physiologically important elastic mechanisms (Fig. 1b–d). At rest length, with no external force, the I-band region of the molecule probably assumes a random-coil configuration[6] (Fig. 1b). As the sarcomere is extended force begins to rise as the molecule is straightened, with little change in secondary or tertiary structure (Fig. 1c). With further stretch, force rises more steeply as the polypeptide conformation in the PEVK region changes from a compact to a more extended configuration (Fig. 1d). At extreme lengths titin detaches from the thick filament (yield point) and the A-band part of the molecule becomes extensible[7] (Fig. 1e). Whether the immunoglobulin or fibronectin

† Present address: Institute of Theoretical and Experimental Biophysics, Puschino, Moscow Region 142292, Russia.

domains can be mechanically unfolded (Fig. 1e) and contribute to extensibility or elasticity is controversial[4,5,8–10].

We tested these proposals by measuring the mechanical properties of individual titin molecules. We tethered a molecule between a glass surface and a polystyrene bead, using antibodies directed against epitopes located near the ends of the molecule. A bead was trapped using optical tweezers and the molecule was stretched by moving a microscope stage horizontally (Fig. 1f–j). We measured force from the displacement of the bead from the trap centre.

We designed the first type of experiment ('dynamic method') to collect data quickly, to minimize stress-relaxation. We stretched the molecule using a triangular wave movement with a frequency of about 2 Hz (Fig. 2, inset). The resulting force–extension curves were highly nonlinear (Fig. 2, continuous curve). We fitted the curves with two polymer models for a chain of contour length L: (1) the freely-jointed chain model (fjc)[11], in which the molecule is considered to consist of rigid segments of average length a, which are freely jointed with respect to neighbouring segments; or (2) the worm-like chain (wlc) model[12], in which the direction of the chain varies continuously, with a persistence length b (which is equivalent to half the segment length at zero external force). Assuming one component of elasticity, there were systematic deviations from the experimental curves (Fig. 2, dots), but excellent fits were obtained assuming two components in series (Fig. 2, circles). The results from both models are summarized in Table 1.

At low force most of the compliance derives from a component with an estimated contour length of 1,000–1,100 nm, with a segment length (fjc) of about 5 nm, or persistence length (wlc) also about 5 nm (component 1, Table 1, first section). The contour length corresponds to the extended length of the molecule excluding the PEVK region (Table 1, second section), and its elasticity then results from the path of the molecule adopting a random coil

Table 1 Lengths of the elastic components of titin

Method	n	L_1 (nm)	d_1 (nm)	L_2 (nm)	d_2 (nm)
Two-component models					
Freely-jointed chain	104	1,070 (125)	5.3 (0.8)	619 (122)	0.35 (0.03)
Worm-like chain	104	1,020 (58)	4.6 (0.9)	416 (45)	0.15 (0.01)
Other studies					
Sequence[3,4]		1,100	4	530–840	0.38
Molecular combing[24]		1,100		150–500	
In situ epitope[4]				500–600	

The first section shows the results of fitting two-component models to the experimental force–extension curves of titin. L is the contour length and d the unitary length of a component. For the freely-jointed chain model d is the segment length, and for the worm-like chain model d is the persistence length. Figures in brackets are s.e.m. Variability in the results may be due to a proportion of the beads having multiple attachments or to tangling or knotting of the titin. The second section shows published results from studies using other methods, where L_1 is the length of the molecule, after subtracting 200 nm for the length excluded by the epitopes in the present study. L_2 is the length of the PEVK region whose size is estimated from its sequence[3,4] and which correlates to a selectively extensible region identified by molecular combining[24] or epitope monitoring *in situ*[4].

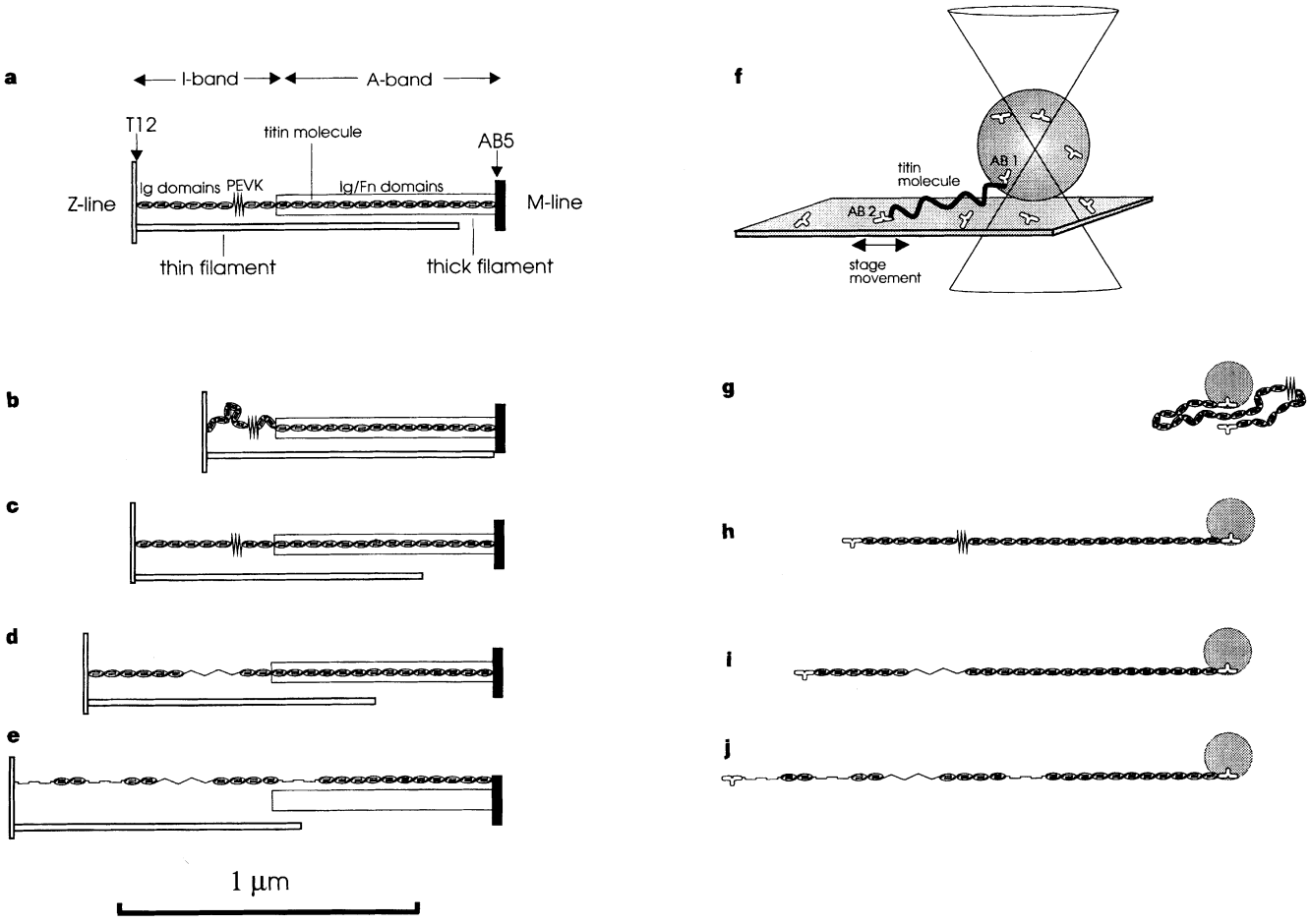

Figure 1 Schematic diagram of mechanisms of elasticity and extensibility of titin *in situ* (**a**–**e**) and in isolated molecules (**f**–**j**). **a**, Structure and location of titin. Ovals represent immunoglobulin and fibronectin domains; there is a total of about 280. Vertical arrows indicate the positions of the antibodies used. **b**, At zero stretch, the titin configuration in the I-band is a random coil and force is zero. **c**, Stretch initially straightens the molecule and force rises. **d**, At moderate stretch, the PEVK region extends. **e**, At extreme stretch, titin detaches from the thick filament. Immunoglobulin and fibronectin domains may also unfold. **f**, Experimental procedure for single molecules. **g**–**j**, Mechanisms of elasticity in single-molecule experiments, corresponding to **b**–**e**.

configuration, with flexibility of 1–2 domains between units. The second component accounts for a greater share of the compliance at higher force (component 2, Table 1, first section). Its contour length is commensurate with the extended length of the PEVK region (Table 1, second section), and its segment length of 0.35 nm is consistent with the predicted repeat per residue of 0.38 nm of fully extended polypeptide.

In the second type of experiment ('static method') we measured the steady-state force–extension relationship by increasing the length of a molecule in steps of about 250 nm, waiting at each stage until stress-relaxation (time constant about 1 s) was nearly complete (inset to Fig. 3a). For small stretches the force–extension behaviour followed the dynamic curve. Stress-relaxation became apparent at some threshold value of force (15–60 pN), after which

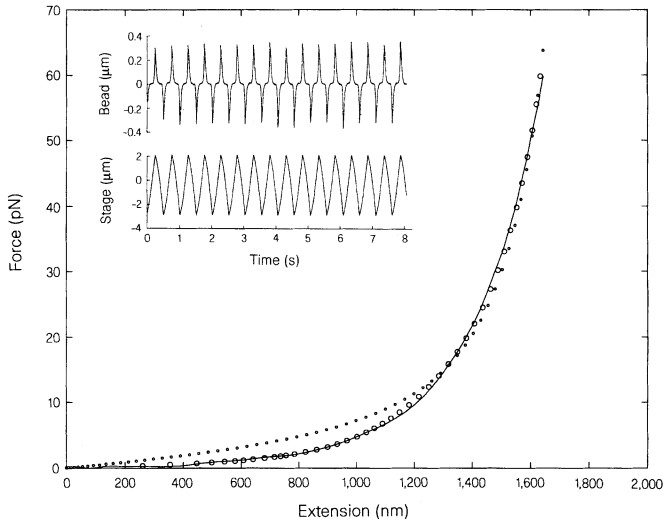

◀ **Figure 2** Dynamic force-extension relationship of titin. Experimental curve from one experiment (continuous curve); fitted using single-component worm-chain model, with $L = 1{,}932$ nm, $b = 0.76$ nm (dots); fitted using two-component worm-chain model, with $L_1 = 1{,}174$ nm, $b_1 = 4.15$ nm, $L_2 = 791$ nm, $b_2 = 0.19$ nm (circles). Fits using the freely-jointed chain model were slightly worse for a single component and equally good for two components. Inset, records of stage movement and resulting bead movement. Extension of the molecule was obtained from the stage movement after subtracting the bead movement and applying a geometric correction; force was obtained from the bead movement, trap stiffness and a geometrical correction (see Methods).

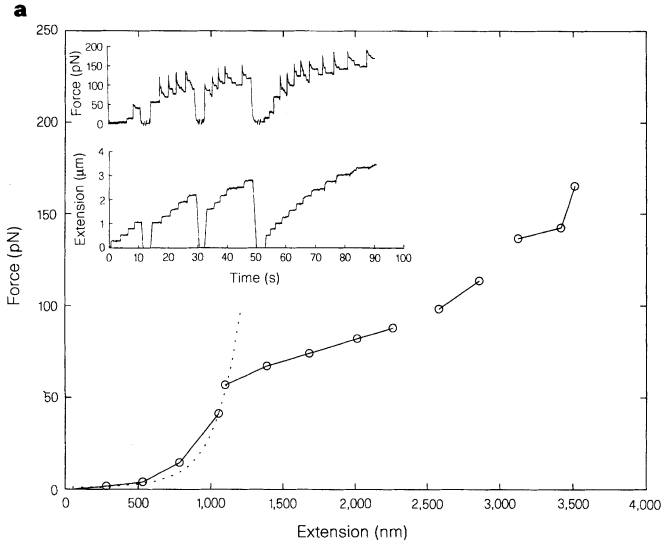

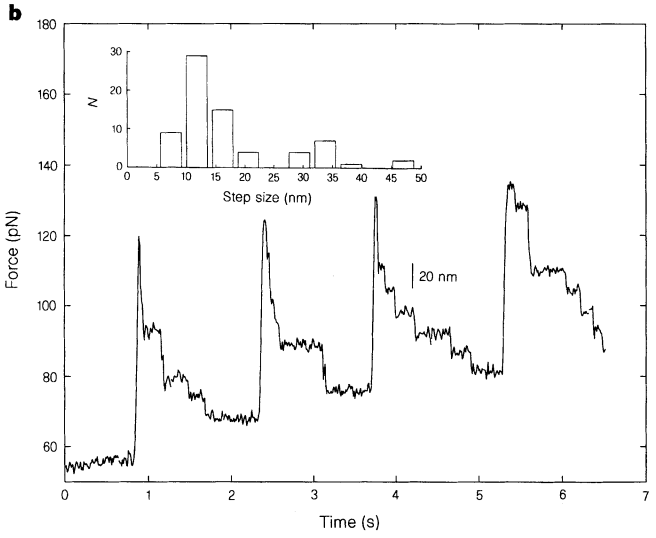

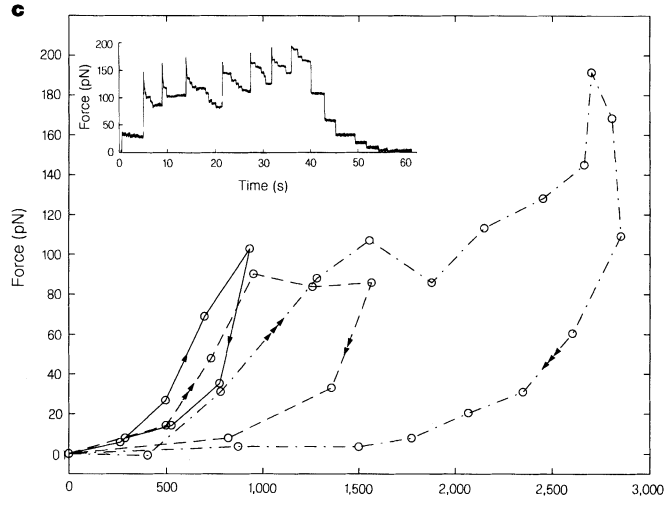

Figure 3 Static force-extension relationship. **a**, Steady-state force-extension relationship (solid lines and circles) derived from three cycles of stretches and releases (records shown in inset). For clarity, only the later non-overlapping points from succeeding cycles are shown. After the end of the last cycle the bead escaped from the trap. The dashed line shows the dynamic force-extension relationship. **b**, Stepwise stress-relaxation (enlargement of part of the record in **a**). The bar shows the scale for the corresponding extension of the molecule, obtained from the slope of the instantaneous force-extension relationship during the rapid length changes. Inset, histogram of step size; the average unitary step size in this experiment was 13 nm, but there was considerable variation between experiments, and the average for all was 19 nm. **c**, Hysteresis. Force-extension relationship from another experiment; complete curves were obtained in three stretch-release cycles. Arrows mark progression around each loop. Inset, force record from third cycle to show unchanging force levels after releases.

the curve was less steep. The average maximum extension achieved in all experiments was 3.2 μm at a force of 110 pN; 5 molecules (out of 22) were extended to 4–7 μm. Indirect evidence for such large extensions has been reported previously[13] and must entail unfolding of immunoglobulin and/or fibronectin domains.

Stress-relaxation occurred in stepwise fashion (Fig. 3b), with a unitary drop in force in the range 3 to 10 pN (or multiples of the unitary value). The corresponding internal extension ('step size'), calculated from the change in force divided by the instantaneous stiffness, was 19 ± 11 nm (mean ± s.d., $n = 821$) from all experiments. The contour length of an unfolded domain was about 35nm (see Methods), agreeing well with the theoretical maximum of 38 nm for domains of 100 residues.

Complete stretch–release cycles show hysteresis loops, which become increasingly wide as the degree of stretch is increased (Fig. 3c), as observed in muscle[7,14]. There was no visible sign of reversal of stress-relaxation following length decrements (inset to Fig. 3c). However, after a completed cycle the subsequent ascending curve usually showed a partial recovery from the previous descending curve, and this was accompanied by stepwise stress-relaxation starting at about the same threshold of force as in the previous cycle (inset to Fig. 3a). This suggests that refolding occurs, but only when the external force has been reduced to a low level. Whether complete recovery can occur after a sufficiently long interval at low force remains to be investigated.

Why do domains unfold? The unperturbed equilibrium constant (K_u) for the folded–unfolded transition determined for a low-stability titin immunoglobulin domain ($\Delta G = 2.6$ kcal mol^{-1}) is about 750 (ref. 15). The half-time of unfolding of an immunoglobulin domain from the related protein twitchin ($\Delta G = 4$ kcal mol^{-1}) is 40 min and the refolding half-time is about 0.5 s (ref. 16). The energy of stretching a domain at a force of 50 pN can be calculated from our experiments to be about 1.8 kcal mol^{-1}. The strain in a domain at 50 pN is about 0.5 nm, presumably sufficient to break inter-chain bonds in the β-sheets of the domains. Allowing for the differences in stability of the titin and twitchin domains, the strain energy could reduce the time constant for unfolding to 1 s, and K_u to 4. In our experiments stretching an unfolded domain to 20 nm will increase its free energy by about 50 kcal mol^{-1}, trapping the unfolded state[9]. For appreciable refolding to occur, the unfolded domain must shorten to near its native folded length, requiring the force to be reduced to a few piconewtons (see Methods). The average stabilities of immunoglobulin and fibronectin domains are comparable[15–18], but variations in stability within both classes will ensure that unfolding is not catastrophic.

At low forces our results are consistent with the model shown in Fig. 1b–d. At high forces yielding is due to domain unfolding, whereas in muscle fibres it is associated with detachment of titin molecules from the thick filament[7]. Perhaps unfolding triggers progressive detachment from the thick filament as a consequence of loss of the tertiary structure presenting the binding site. Does unfolding contribute to extensibility in the physiological range of sarcomere lengths? Muscle fibres exhibit stress-relaxation and hysteresis well below the length at which yielding occurs[7,14] and this might entail a limited amount of unfolding; it is thus conceivable that the immunoglobulin domains act as shock absorbers.

Note added in proof: Gaub, Bustamante and colleagues have independently reported similar findings[25,26]. □

Methods

Bead preparation. Antibodies were covalently coupled to aldehyde-polystyrene latex microspheres, diameter 1.1 μm: 10 μl of the bead suspension (~7.7×10^{10} ml^{-1}) were diluted to 1 ml with 10 mM HEPES buffer, pH 7.5, and 10–50 μl of antibody solution (cell supernatant) was added. After 30 min incubation at room temperature with constant stirring, 10–20 μl BSA solution (10 mg ml^{-1}) in HEPES buffer was added for a further 20 min. The suspension was then sonicated, diluted to 10 ml with 50 mM Tris, 10 mM β-mercaptoethanol solution, pH 7.5, and centrifuged at 10,000*g* for ~10 min. Washing in the Tris buffer was repeated before the beads were suspended in 1 ml 0.3 M KCl, 0.1 mM NaN_3, 1 mM EGTA, 0.1 mM DTT, 10 mM histidine, pH 7.5.

Cell-surface preparation. A flow cell (internal volume ~50μl) was made from a clean glass coverslip, coated with a thin film of nitrocellulose and a microscope slide, separated by two strip fragments of coverslip (attached by Vaseline). Incubations, each 10 min, were performed at room temperature sequentially as follows: antibody solution (cell supernatant); BSA (10 mg ml^{-1}) in 0.3 M KCl, pH 7.5; titin (0.1 mg ml^{-1} in 0.3 M KCl, pH 7.5, prepared from rabbit back muscle[19]) containing 5 mg ml^{-1} BSA; bead suspension. The final solution was 0.3 M KCl. In the experiments described the antibodies used bind ~100 nm from the M- (AB5; ref. 20) and Z-lines (T12 (ref. 12) or DB1; J.T., unpublished data) *in situ*. Preliminary experiments using a wide variety of antibodies showed that the displacement of beads with a roughly 1-pN force, produced by fluid flow, depended on the distance between epitopes determined *in situ*, thus validating the method.

Density of titin and antibodies on the bead and coverslip. Rough calculations of antibody density on the surfaces, allowing for the likely binding efficiency towards titin, give upper limits for the density of bound titin molecules on the coverslip of 2 per μm^2, and ~8 competent binding sites per bead. The observed density of tethered beads was very much lower than this, about 100–1,000 per mm^2, and this was not increased by longer incubation times of the beads. Thus, it is likely that most beads were attached by a single linkage.

Equipment. Most of the optical-tweezers technique used has been described previously[22]. The apparatus was based on a modified inverted microscope (Zeiss Axiovert), using a 2W Nd-YLF laser, 1.047 μm (TFR, SpectraPhysics), with a × 63 Planapo NA 1.4 objective. The slide was mounted on a piezoelectric transducer (pzt)-operated stage (natural frequency ~100 Hz) equipped with capacitance gauge transducers. Experimental data were digitized using a PC with an analog-to-digital converter (National, Labview), usually at a sampling frequency of 2 kHz. Trap stiffness was determined from the root-mean-square deviation of the brownian motion of a trapped bead, or from the corner frequency of brownian noise, or the response to a sine-wave input into a stage pzt, with a trapped bead about 5 μm above the coverslip surface.

Dynamic force–extension data. Having trapped a bead and centred it by trial and error, a triangular wave was applied to one pzt, and the quadrant detector and capacitance gauge outputs were recorded. Data were processed as follows: calibrations for the capacitance gauge and the detector were applied and corrections were made for the nonlinearity of the detector and for the nonlinearity of force produced by the trap. Five to sixteen triangular wave sweeps were averaged and filtered at 100 Hz. The four quadrants of data from the triangular wave were averaged and converted into extension and force, assuming that the bead was free to rotate, and correcting for the geometry of the bead and molecule. Analysis programs were written using Matlab.

Static force–extension data. The method used was similar to that described for the dynamic force–extension data, except that length changes were applied using the digital-to-analog output from a PC, giving ramp-faced steps (velocity 250 nm s^{-1}), and the pzt-operated stage was servo-controlled. Beads tended to detach at high maintained force, and the most complete experiments entailed a compromise with the time allowed for the steady state to be established after a stretch (Fig. 3). The bead centring was checked at the end of an experiment, showing that in most cases slippage was negligible.

Polymer models. Least-squares fits to the experimental force-extension data were made for the freely-jointed chain model[11] and the worm-like chain model[12] (using the interpolation formula given in ref. 23), allowing all the parameters to vary. A Simplex method (Matlab) was used. The force–extension curve for an unfolded domain was obtained by subtraction of the dynamic curve from the release section of a hysteresis curve, weighted for the number of unfolded domains. The resultant curve was then fitted with a single component freely-jointed chain model to obtain the contour length.

Received 4 March; accepted 14 April 1997.

1. Trinick, J. Cytoskeleton: titin as a scaffold and spring. *Curr. Biol.* **6,** 258–260 (1996).
2. Maruyama, K. Connectin, an elastic protein of striated muscle. *Biophys. Chem.* **50,** 73–85 (1994).
3. Labeit, S. & Kolmerer, B. Titins: giant proteins in charge of muscle ultrastructure and elasticity. *Science* **270,** 293–296 (1995).
4. Linke, W. A. *et al.* Towards a molecular understanding of the elasticity of titin. *J. Mol. Biol.* **261,** 62–71 (1996).
5. Gautel, M. & Goulding, D. A molecular map of titin/connectin elasticity reveals two different mechanisms acting in series. *FEBS Lett.* **385,** 11–14 (1996).

6. Higuchi, H., Nakauchi, Y., Maruyama, K. & Fujime, S. Characterization of α-connectin from striated muscle by dynamic light scattering. *Biophys. J.* **65,** 1906–1915 (1993).
7. Wang, K., McCarter, R., Wright, J., Beverly, J. & Ramirez-Mitchell, R. Viscoelasticity of the sarcomere matrix of skeletal-muscles: the titin-myosin composite filament is a dual-stage molecular spring. *Biophys. J.* **64,** 1161–1177 (1993).
8. Soteriou, A., Clarke, A., Martin, S. & Trinick, J. Titin folding energy and elasticity. *Proc. R. Soc. Lond. B* **254,** 83–86 (1993).
9. Erickson, H. P. Reversible unfolding of fibronectin type-III and immunoglobulin domains provides the structural basis for stretch and elasticity of titin and fibronectin. *Proc. Natl Acad. Sci. USA* **91,** 10114–10118 (1994).
10. Politou, A. S., Thomas, D. J. & Pastore, A. The folding and stability of titin immunoglobulin-like modules, with implications for the mechanism of elasticity. *Biophys. J.* **69,** 2601–2610 (1995).
11. Flory, P. J. in *Statistical Mechanics of Chain Molecules* 316–304 (Hanser, Munich, 1989).
12. Fixman, M. & Kovac, J. Polymer conformational statistics. III. Modified Gaussian models of stiff chains. *J. Chem. Phys.* **56,** 1564–1568 (1973).
13. Kellermayer, M. S. Z. & Granzier, H. L. Elastic properties of single titin molecules made visible through fluorescent F-actin binding. *Biochem. Biophys. Res. Comm.* **221,** 491–497 (1996).
14. Linke, W. A., Bartoo, M. I., Ivemeyer, M. & Pollack, G. H. Limits of titin extension in single cardiac myofibrils. *J. Muscle Res. Cell Motil.* **17,** 425–438 (1996).
15. Politou, A. S., Gautel, M., Pfuhl, M., Labeit, S. & Pastore, A. Immunoglobulin-type domains of titin: same fold, different stability? *Biochemistry* **33,** 4730–4737 (1994).
16. Fong, S. *et al.* Structure and stability of an immunoglobulin superfamily domain from twitchin, a muscle protein of the nematode *Caenorhabditis elegans. J. Mol. Biol.* **264,** 624–639 (1996).
17. Litvinovich, S. V., Novokhatny, V. V., Brew, S. A. & Ingram, K. C. Reversible unfolding of an isolated heparin and DNA binding fragment, the first type III module from fibronectin. *Biochim. Biophys. Acta* **1119,** 57–62 (1992).
18. Plaxco, K. W., Spitzfaden, C., Campbell, I. D. & Dobson, C. M. Rapid refolding of a proline-rich all-beta-sheet fibronectin type-III module. *Proc. Natl Acad. Sci. USA* **93,** 10703–10706 (1996).
19. Soteriou, A., Gamage, M. & Trinick, J. A survey of the interactions made by the giant protein titin. *J. Cell Sci.* **104,** 119–123 (1993).
20. Whiting, J., Wardale, J. & Trinick, J. Does titin regulate the length of muscle thick filaments. *J. Mol. Biol.* **205,** 263–268 (1989).
21. Fürst, D. O., Osborn, M., Nave, R. & Weber, K. The organisation of titin filaments in the half-sarcomere revealed by monoclonal-antibodies in immunoelectron microscopy: a map of ten nonrepetitive epitopes starting at the Z-line extends close to the M-line. *J. Cell Biol.* **106,** 1563–1572 (1988).
22. Simmons, R. M., Finer, J. T., Chu, S. & Spudich, J. A. Quantitative measurements of force and displacement using an optical trap. *Biophys. J.* **70,** 1813–1822 (1996).
23. Bustamante, C. Entropic elasticity of λ-phage DNA. *Science* **265,** 1599–1600 (1994).
24. Tskhovrebova, L. & Trinick, J. Direct visualization of extensibility in isolated titin molecules. *J. Mol. Biol.* **265,** 100–106 (1997).
25. Rief, M., Gautel, M., Oesterhelt, F., Fernandez, J. M. & Gaub, H. E. Reversible unfolding of individual titin Ig-domains by AFM. *Science* (in the press).
26. Kellermayer, M. S. Z., Smith, S. B., Granzier, H. L. & Bustamante, C. Folding-unfolding transitions in single titin molecules characterized with force-measuring laser tweezers. *Science* (in the press).

Acknowledgements. We thank M. Gautel, W. Gratzer, P. Knight, G. Offer, A. Pastore and D. Thomas for discussions and advice. Supported by BBSRC and NIH (J.T.), MRC (J.A.S. & R.M.S.) and the Human Frontier Science Program (R.M.S.).

Correspondence and requests for materials should be sent to R.M.S. (e-mail: r.simmons@kcl.ac.uk).

Crystal structure of ICAM-2 reveals a distinctive integrin recognition surface

José M. Casasnovas*, Timothy A. Springer*, Jin-huan Liu†‡, Stephen C. Harrison†§ & Jia-huai Wang†‡

** The Center for Blood Research, Harvard Medical School, Department of Pathology, 200 Longwood Avenue, Boston, Massachusetts 02115, USA*

† Department of Molecular and Cellular Biology, and § Howard Hughes Medical Institute, Harvard University, 7 Divinity Avenue, Cambridge, Massachusetts 02138, USA

Recognition by integrin proteins on the cell surface regulates the adhesive interactions between cells and their surroundings[1,2]. The structure of the 'I' domain that is found in some but not all integrins, has been determined[3,4]. However, the only integrin ligands for which structures are known, namely fibronectin and VCAM-1 (refs 5–7), are recognized by integrins that lack I domains. The intercellular adhesion molecules ICAM-1, 2 and 3 are, like VCAM-1, members of the immunoglobulin superfamily (IgSF), but they are recognized by an I domain-containing integrin, lymphocyte-function-associated antigen 1 (LFA-1, or CD11a/CD18). Here we present the crystal structure of the extracellular region of ICAM-2. The glutamic acid residue at position 37 is critical for LFA-1 binding and is proposed to coordinate the Mg^{2+} ion in the I domain; this Glu 37 is surrounded by a relatively flat recognition surface and lies in a β-strand, whereas the critical aspartic acid residue in VCAM-1 and fibronectin lie in protruding loops. This finding suggests that there are differences in the architecture of recognition sites between integrins that contain or lack I domains. A bend between domains 1 and 2 of ICAM-2 and a tripod-like arrangement of *N*-linked glycans in the membrane-proximal region of domain 2 may be important for presenting the recognition surface to LFA-1. A model of ICAM-1 based on the ICAM-2 structure provides a framework for understanding its recognition by pathogens.

The extracellular fragment of ICAM-2 containing the two predicted IgSF domains was expressed in lectin-resistant CHO Lec.3.2.8.1 cells[8] to obtain a homogeneous, high-mannose, *N*-linked glycoform. Crystallization trials were done with native and endoH-treated ICAM-2, and crystals were obtained only with the native protein. The structure was determined by multiple isomorphous replacement (MIR) and refined by XPLOR (see Methods and Table 1).

ICAM-2 has two domains with an immunoglobulin(Ig)-like fold (Fig. 1a). The molecule resembles a hockey stick, with a bend of 35° and a rotation of 152° between the N-terminal, membrane-distal domain 1 (D1), and the C-terminal, membrane-proximal domain 2 (D2), defined by superposition of the Ig framework. With domain 2 oriented perpendicular to the membrane, the edge of the two β-sheets formed by β-strands C and D in domain 1 faces outwards.

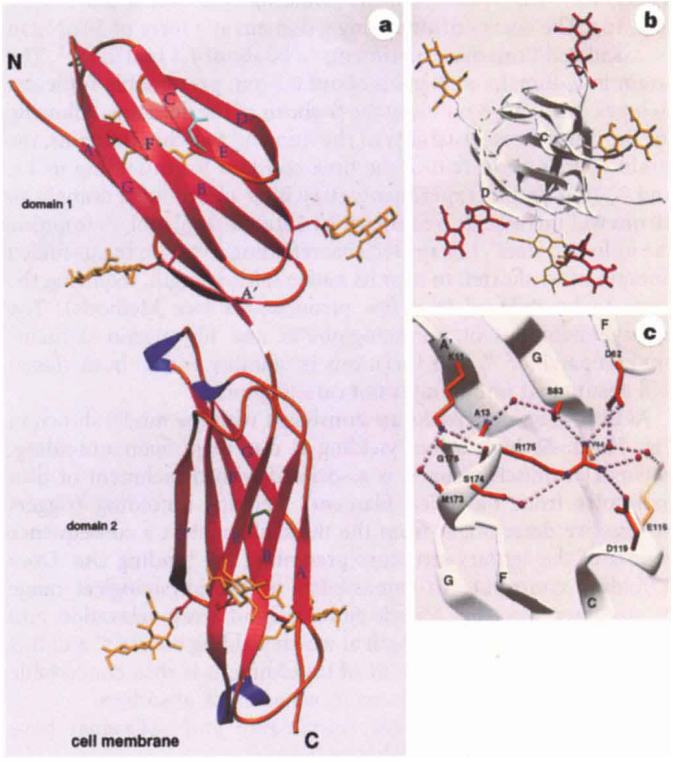

Figure 1 The crystal structure of ICAM-2. **a**, Ribbon diagram with β-strands in red, α-helix in blue and coil in orange. The last residue of domain 1 (Tyr 85) is white. *N*-linked sugars (yellow), Glu 37 in strand C of domain 1 (light blue) and disulphide bonds (green) are included. **b**, View from the top of domain 1 towards the membrane. Sugars linked to domains 1 and 2 are yellow and red, respectively. **c**, Hydrogen bonds between residues in domain 1 (top) and 2 (bottom). Nitrogen and oxygen atoms are in blue and red, respectively. Water molecules are shown as red spheres. Prepared with Ribbons[29].

‡ Present address: Dana-Farber Cancer Institute (J.-h.L. and J.-h.W.) and Children's Hospital (J.-h.W.), Harvard Medical School, 44 Binney Street, Boston, Massachusetts 02115, USA.